Title
Surface energy minimizing configurations for axisymmetric microparticles

Journal
Journal of Engineering Mathematics, 134(1)

ISSN
0022-0833

Authors
Ha, Kyung
de Rutte, Joseph
Di Carlo, Dino
et al.

Publication Date
2022-06-01

DOI
10.1007/s10665-022-10216-9

Peer reviewed

J Eng Math (2022) 134:2
https://doi.org/10.1007/s10665-022-10216-9

Surface energy minimizing configurations for axisymmetric microparticles

Kyung Ha · Joseph de Rutte · Dino Di Carlo · Andrea L. Bertozzi

Received: 4 February 2021 / Accepted: 11 March 2022 / Published online: 5 May 2022

Abstract An important area of microfluidics is the creation and manipulation of small droplets. This is commonly done using microchannels or electrowetting. Recently a new method is proposed to create templated droplets using amphiphilic microparticles. These particles are observed to hold nearly equal volumes of aqueous liquid when dispersed in an oil–water mixture. However a theory for this behavior is lacking. In this paper, we present a mathematical model based on minimizing the surface tension energy of a system of axisymmetric particles. By analyzing this model, we demonstrate that certain key properties of the particle guarantee the formation of small droplets within a volume range unique to the particle.

Keywords Droplets · Microfluidics · Surface energy minimizing configurations · Surface tension · Volume constraint optimization

1 Introduction

The creation and manipulation of fixed-sized miniature droplets is an important area of study in microfluidics, enabling highly sensitive biological and chemical assays [1]. A benefit of such technology is that by compartmentalizing a larger volume into sub-components, individual cells or molecules can be analyzed more precisely. This is

K. Ha (✉)
Department of Mathematics, University of California Los Angeles, Los Angeles, CA 90095, USA
e-mail: kyungha@g.ucla.edu

J. de Rutte
Department of Bioengineering, University of California Los Angeles, Los Angeles, CA 90095, USA
e-mail: jderutte@ucla.edu

D. Di Carlo
Department of Bioengineering and Department of Mechanical and Aerospace Engineering, University of California Los Angeles, Los Angeles, CA 90095, USA
e-mail: dicarlo@ucla.edu

A. L. Bertozzi
Department of Mathematics and Department of Mechanical and Aerospace Engineering, University of California Los Angeles, Los Angeles, CA 90095, USA
e-mail: bertozzi@math.ucla.edu

because the secretion of molecules from a cell, or the products of reactions of individual molecules, can quickly accumulate to high concentrations when confined in small volumes. Conventional technologies are focused on droplet formation and manipulation via flow in microchannels [2–4] or in electrowetting devices [5–7]. Another approach, recently developed, is the creation of microscale solid drop-carrier particles (DCPs)- with complex geometries and hydrophilic parts that allow for the capture of uniform-sized droplets simply by having favored conditions related to their surface energy [1,8–10] (Fig. 1). These DCPs can result in stable isolated volumes on the nanoliter or sub-nanoliter scale when simply mixed. Molecules accumulating in these small volumes at high concentrations can also bound to the DCP, enabling analysis with standard equipment such as flow cytometers. This can lead to "lab on a particle" technologies in which experiments can be done on thousands of individual cells, to study phenomena at the cellular level.

However a theory behind this new technology is lacking. To develop this theory, we formulate an energy minimization problem of the system and ask two questions: (a) the optimal energy configuration for specific DCP designs; and (b) for a multi-DCP system. We calculate the energy-related to surface tensions only, since it is the dominant contributor at the microscale compared to other forces, for example, buoyancy.

Finding a configuration that minimizes surface tension while maintaining a certain volume is a classical problem in geometry [11,12]. One especially well-documented case is the problem of a liquid bridge between two axisymmetric surfaces. Common examples of such surfaces are spheres [13–15] and flat planes, including both infinitely large planes [16–20], and finite size flat surfaces [21–28]. One work considers one side finite and the other infinite [29]. Results with more general shapes are also well documented in [30]. Additionally, recent work explores the distribution of fluid drops emerging from networked orifices [31–33].

In this paper, we investigate surface energy minimizing configurations for more complex axisymmetric DCPs (Fig. 2) for which there exists recent experimental data [9,34]. In this case, the ensuing minimization problem is reduced to a 1D problem and is relatively straightforward so rigorous results are derived. Moreover, such symmetry often corresponds to simplified manufacturing technologies for producing such DCPs in bulk. It is possible to achieve these energy minimizing configurations without the axisymmetric assumption using 3D simulations as in [1]. However, this is computationally expensive compared to 1D simulations. Once we obtain the configuration of a single DCP we study the multi-DCP system and its minimal energy distribution of a fixed volume of fluid. We develop a theory for the minimum energy configuration of multi-DCP systems and perform simulations of pairwise interactions. This will help us develop ideas for efficient DCP designs.

Our paper is organized as follows. In Sect. 2, we explore three DCP configurations of interest: planar surfaces, hollow spheres, and hollow cylinders (Fig. 2). We deduce the shape of the energy minimizing configuration and

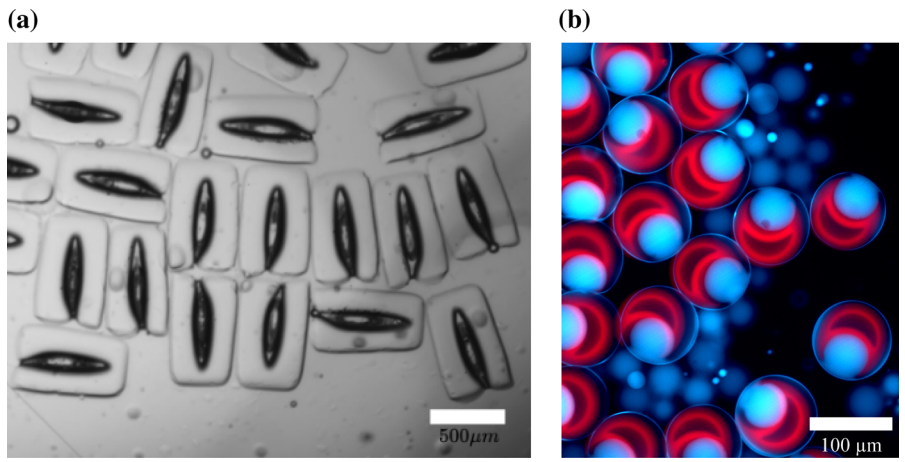

Fig. 1 Experimental photos of "dropicles". In both images, water is captured inside DCPs which are surrounded by oil. In **a** the DCPs are those in [1], which are not axisymmetric and have a fully 3D structure. The DCPs in **b** are those in [9] and are shaped as in Fig 2b. **b** is a false-color image, with the DCP colored in red and water colored in blue. The surrounding oil appears dark

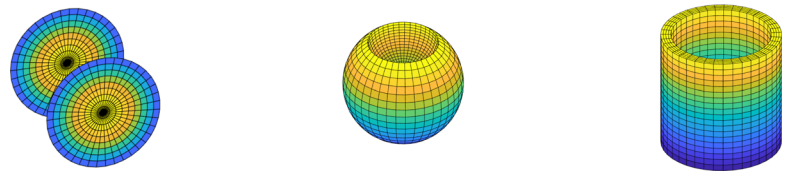

(a) Two parallel flat planes **(b)** Hollow sphere **(c)** Hollow Cylinder

Fig. 2 Shapes of axisymmetric solids. **a** cross-section of **b** and **c** are shown in Fig. 3b and 3c respectively

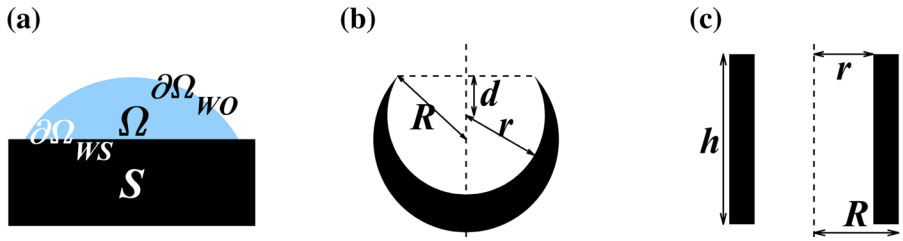

Fig. 3 Examples of axisymmetric solid surfaces. **a** is a droplet (blue) on a flat surface (black). **b** and **c** are cross-sections of a hollow sphere and a hollow cylinder, respectively, with the axis of symmetry shown as a dotted vertical line. The solid phases are colored in black. In **b**, R and r are the radii of the outer and inner spheres respectively, and d is the offset between the tip of the DCP and the center of the inner sphere. In the figure the parameters are $R = 1.18$, $r = 1$, and $d = 0.5$. In **c**, h is the height and R and r are the inner and outer radius of the cylinder. In the figure the parameters are $R = 0.9$, $r = 0.7$ and $h = 3$

calculate the volume-energy graph for each DCP. In Sect. 3, we develop a rigorous theory regarding the minimal configuration for a multi-DCP system. We can predict the minimal energy distribution of multi-DCP systems by observing properties of the volume-energy graph of a single water-DCP complex. In Sect. 4, we simulate the interaction between two and multiple DCPs. The simulation verifies the results in Sect. 3 and also suggests guidelines for DCP design. Throughout the paper, we follow the terminology in [1,8–10], by denoting the target liquid as water, the surrounding liquid as oil. We likewise denote the water-DCP complex as a "dropicle" (drop+particle).

2 Energy minimizing surfaces

In this section, we focus on finding the minimal energy surface configuration for a given DCP and volume. By repeating these calculations for different volumes, we draw a volume-energy graph ($V - E$ graph) of a DCP.

Denote the fixed solid region by S, the finite volume of water by Ω, the water-solid interface by $\partial\Omega_{WS}$ and the water-oil interface by $\partial\Omega_{WO}$. Note that $\partial\Omega = \partial\Omega_{WS} \cup \partial\Omega_{WO}$ (Fig. 3a). The interfacial tension energy of the dropicle is

$$\begin{aligned} E(\Omega) &= \sigma_{WO}|\partial\Omega_{WO}| + \sigma_{WS}|\partial\Omega_{WS}| + \sigma_{OS}(|\partial S| - |\partial\Omega_{WS}|) \\ &= \sigma_{WO}|\partial\Omega_{WO}| + (\sigma_{WS} - \sigma_{OS})|\partial\Omega_{WS}| + \sigma_{OS}|\partial S|, \end{aligned} \tag{1}$$

where $|\partial S|$ is the surface area of the solid, $|\partial\Omega_{WO}|$ and $|\partial\Omega_{WS}|$ are the water-oil and water-solid surface areas of Ω respectively, σ_{WS}, σ_{WO} and σ_{OS} are surface tensions between water-solid, water-oil and oil-solid respectively. We consider DCPs with a partial wetting hydrophilic solid phase, i.e.

$$\sigma_{WO} > \sigma_{OS} - \sigma_{WS} > 0. \tag{2}$$

Throughout this paper we use the surface tensions values $\sigma_{WO} = 1$, $\sigma_{WS} = 0.1$, and $\sigma_{OS} = 0.9$, unless stated otherwise. This choice is consistent with the use of hydrophilic materials for the DCPs in the experiments [1,8,9]. Qualitatively the results do not change much with modest variation in these parameters (c.f. Sect. 4.2). We note that the last

term in (1) only depends on ∂S and is independent of the water domain Ω so we ignore it as far as the minimal energy calculation is concerned. Also, we note that the energy equation does not take any dynamics around the dropicle into account, and therefore our model is a static fluid model. We need to find an Ω that minimizes the energy (1) under the volume constraint $|\Omega| = V$. Since the ratio of surface energies determine the static problem the energy can be dimensionless. Throughout this paper, we assume that for each dropicle Ω is an open bounded and connected domain.

Solving (1) is well documented in [30] chapter 2. The minimizing surface is a constant mean curvature surface, with a prescribed contact angle α satisfying,

$$cos\alpha = (\sigma_{OS} - \sigma_{WS})/\sigma_{WO} \tag{3}$$

called the Duprè–Young condition for smooth solid surfaces. For sharp surfaces (e.g. tips of Fig. 3b) we consider a range of contact angles rather than a single choice. The range depends on α and the angle of the sharp solid. A way to understand this is by smoothing the sharp surface locally and applying the condition in (3) to a specific point in the smoothed area.

The physical cases of interest here are all axisymmetric connected solids (Fig. 2b and 2c), with simply connected axisymmetric water domains. Under these assumptions, the water-oil interface $\partial\Omega_{WO}$ of the problem (1) is part of a sphere.

Theorem 1 *Assume the surface tensions satisfy the partial wetting condition* (2) *and the solid is axisymmetric and connected. Also, assume that the water domain is bounded, simply connected and axisymmetric. Then the water-oil interface that minimizes* (1) *is part of a sphere.*

Proof This theorem summarizes results discussed in detail in [30] Chapter 2.4.4. □

The rest of this section uses this theoretical result to compute the energy-volume curves for the DCP shapes of interest. We start with the classical case of two parallel planes, which are well-studied in the literature, to contrast with the hollow DCP shapes that are less well-studied.

2.1 Two parallel planes

The parallel plane case is well-known [19]. In this case, there are two types of geometries to consider for Ω: (a) a droplet that only touches one of the planes or (b) a bridge between the two planes.

Spherical cap: For the case where the water only comes into contact with one of the planes, since the surface is connected and axisymmetric, we obtain a spherical cap as the minimizer by applying Theorem 1. The size and shape of the sphere are decided from the volume constraint and the Duprè–Young condition.

Liquid bridge : For the case when water connects both planes of distance $2a$, using calculus of variations, it is known [19] that an axisymmetric bridge forms with shape profile $f(x)$ between $-a$ and a satisfying,

$$\frac{f''}{(1+(f')^2)^{3/2}} - \frac{1}{f(1+(f')^2)^{1/2}} = 2H, \tag{4}$$

where H is the Lagrange multiplier corresponding to the volume constraint, with Neumann boundary conditions

$$f'(-a) = \frac{\sigma}{\sqrt{1-\sigma^2}}, \quad f'(a) = -\frac{\sigma}{\sqrt{1-\sigma^2}}, \tag{5}$$

where $\sigma = (\sigma_{WS} - \sigma_{OS})/\sigma_{WO}$ (Fig. 4b). The boundary conditions that arise are identical to those given by the Duprè–Young condition.

Fig. 4a shows the $V - E$ graph of different configurations. The $V - E$ graph for the spherical cap is calculated by minimizing (1) under the volume constraint using basic calculus, while the liquid bridge is calculated by solving (4) and (5) numerically using the shooting method [35] for a given range of H. Depending on the volume of water, the minimum energy configuration is either the spherical cap for small volumes or liquid bridge for large volumes. The transition happens where the blue dotted line and red dashed line intersect. The liquid bridge does not extend to zero volume as it requires a finite amount of water to form a bridge. Notice that we do not need to consider the case which we have multiple spherical caps. This is because the lowest energy state within the subcategory of spherical caps is the one with a single cap (Theorem 2).

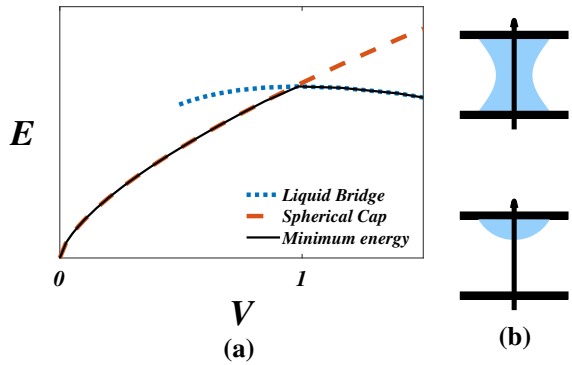

Fig. 4 Parallel plane dropicles. **a** is the $V - E$ graph of water droplets with different geometries. They are a liquid bridge on the parallel plane, and a spherical cap on one side, with their cross-sections shown in **b** respectively. The minimum energy curve is represented as a black solid line. The unit volume is $(2a)^3$ where $2a$ is the distance between the parallel planes

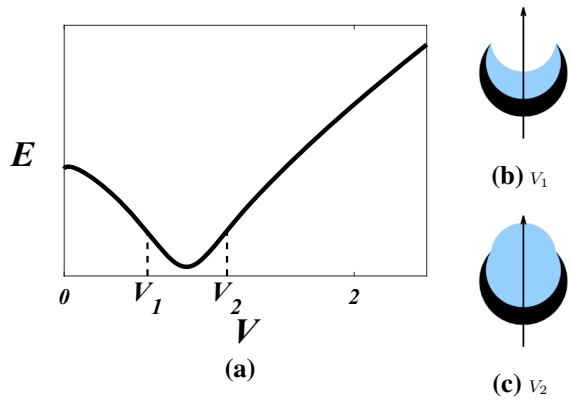

Fig. 5 Hollow sphere dropicle. **a** is the $V - E$ graph of the hollow sphere DCP. The minimum is obtained when the water-oil interface is flat. **b** and **c** are cross-sections of the dropicle through the axisymmetric axis. The volume contained in each image corresponds to the volumes V_1 and V_2 indicated on the graph. The parameters of the DCP are those given in Fig. 3b. The unit volume is given as $V_{IS} = \frac{4}{3}\pi r^3$

2.2 Hollow sphere

Next, we consider a DCP shaped as in Fig. 3b, a larger sphere with a smaller inner sphere carved out to form an exposed cavity, which we call the hollow sphere. Assuming that the water-oil surface is axisymmetric, by Theorem 1, the shape of the minimal energy surface is a spherical cap with a curvature that can differ from those of the DCP surfaces. We can calculate the $V - E$ graph analytically following [36,37]. However, instead of using this analytic method, we follow a numerical method as outlined below.

1. For a given water volume and circular triple junction (contact line), there exists one spherical surface. We compute the surface energy of the entire system for this chosen contact line.
2. Fix the volume and find the contact line which minimizes the energy of the system.
3. Repeat the calculation for different volumes.

Fig. 5a shows the $V - E$ graph of a hollow sphere DCP with cross-section shown in Fig. 3b. For small volumes of water, we see a decrease in energy as the volume increases, until the water volume is large enough so that it reaches the outer edge of the hollow sphere and forms a flat surface. Two special volumes of interest are V_1, the smallest volume for which the water droplet reaches the edge of the hollow sphere, and V_2, the largest such volume. Once the water volume exceeds V_2 the energy minimizing configuration wets the outside sphere. When the contact

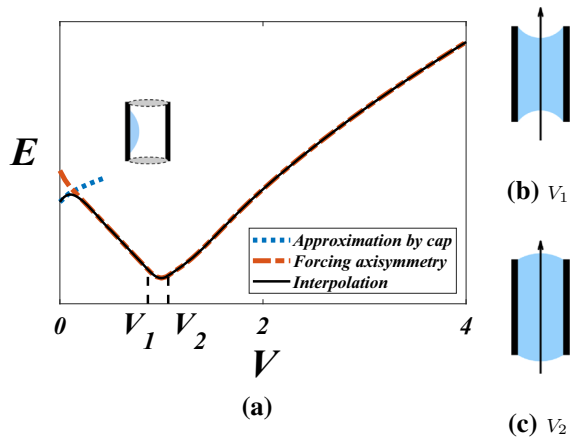

Fig. 6 Hollow cylinder dropicle. **a** is the $V - E$ graph of the hollow cylinder DCP given in Fig. 3c. The red line represents the $V - E$ graph when axisymmetry is forced. The minimum energy is obtained when the top and bottom water-oil interfaces are flat. The blue line represents an approximation of the non-axisymmetric surface by a spherical cap and the black line is an interpolation of these two energies which is an approximation of the true $V - E$ graph. **b** and **c** are cross-sections of the dropicle through the axisymmetric axis with water volume V_1 and V_2. The unit volume is given as the volume of the inner cylinder $V_{IC} = \pi r^2 h$

line is away from the sharp tip, the Duprè–Young condition holds for the surface. However, for the sharp corner, the surface does not necessarily satisfy the condition.

2.3 Hollow cylinder

The DCP we consider in this section is an empty cylinder with a finite wall width (Fig. 3c), which we call a hollow cylinder. We assume that the water-oil surface is axisymmetric about the axis of the cylinder. By Theorem 1, the shape of the water-oil surface is part of a sphere. Similar to Sect. 2.2, we calculate the $V - E$ graph by determining the minimum energy configuration of the top and bottom water-oil interfaces that contain the given volume (red line in Fig. 6a). As in Fig. 5a, V_1 and V_2 denote the smallest and largest volumes on which the contact line of the droplet are the edges of the inner cylinder. When the contact line is away from the edges, the Duprè–Young condition holds for the energy minimizing configuration, but not necessarily for the sharp corners.

For a sufficiently small volume, the water domain that minimizes the energy of the system (1) is not axisymmetric - the drop attaches to the inside wall of the cylinder. It can then be approximated by a spherical cap on a flat plane (blue line). In this paper we assume that the cylinder is narrow enough ($r < h$ in Fig. 3c), so that the minimum energy configuration is axisymmetric for large enough water volumes ($V > 0.2$ in Fig. 6a). For such DCPs, these small volumes are not relevant to large scale systems with multiple DCPs exchanging fluid, as in the following sections. For these reasons, we smooth the axisymmetric $V - E$ graph at small volumes to simplify the analysis, which requires continuity of E' with respect to E. The case of an extremely flat cylinder is addressed experimentally in [8]. For such DCPs, partial filling is typically not axisymmetric, requiring careful numerical simulation of the fully 3D energy minimization problem, as was carried out in [1] for another non-axisymmetric DCP shape. Finally we mention that discontinuities in E' typically result from topology changes in the minimizing configuration, when V is varied, such as in the example in Fig 4. The regime of interest to us for the cylinders and hollow spheres does not involve topology changes and thus can be addressed with arguments that assume continuity of E'.

3 Rigorous theory of energy minimizing surface

In this section, we answer how the $V - E$ graphs can be used to analyze the interactive behavior between dropicles. We develop a theory for the water distribution that minimizes energy among multiple dropicles. First we consider

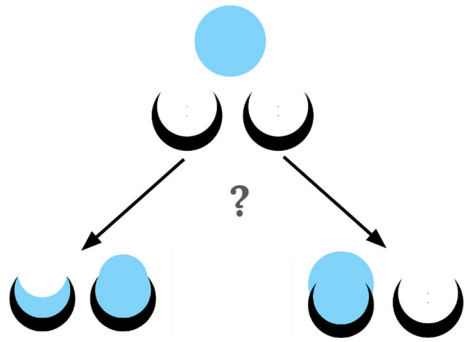

Fig. 7 What is the optimal way to split a volume of water between two DCPs?

two identical DCPs and a fixed total volume of water. The first derivative of the graph is key in understanding how to split the water between the DCPs to achieve the energy minimum. Extending this idea we prove a theorem for systems with more than two DCPs. Throughout this paper, we assume each dropicle contains only one DCP, i.e. no two DCPs are connected by the same water droplet. In real physical systems, sometimes one observes coalescence of these dropicles. However, this is beyond the scope of our current analysis.

3.1 Droplet splitting between two DCPs

For a DCP along with its $V - E$ graph, $E(V)$, we address the question of the optimal water distribution between two identical DCPs, given a fixed total water volume V_T. Does the water droplet split into two smaller drops or remain intact (Fig. 7)? We formulate this as an optimization problem

$$\overline{V} = \text{argmin}_{0 \le V \le V_T}\{E(V) + E(V_T - V)\}. \tag{6}$$

This optimization problem minimizes the sum of the static energy function $E(V)$. For this section, we only consider functions $E(V)$ that are continuously differentiable.

By the symmetry of the problem, we obtain two $\overline{V}$ for a minimum energy distribution. The smaller volume of the two, which we denote as V_S,

depends on the total volume V_T and satisfies either $V_S = 0$ or

$$E'(V_S) = E'(V_T - V_S). \tag{7}$$

3.1.1 Convex and Concave $V - E$ graphs

We first note that for convex and concave $E(V)$, the result is a simple application of convexity. We state this as a theorem below.

Theorem 2 *Assume $E(V) \in \boldsymbol{C}^1[0, \infty)$. If $E(V)$ is a convex function, $V_S = V_T/2$. If $E(V)$ is a concave function, $V_S = 0$. If $E(V)$ is strictly convex or strictly concave, the minimizer is unique.*

Proof If $E(V)$ for $0 \le V \le V_T$ is a convex function the total energy function $E(V) + E(V_T - V)$ is also a convex function. The minimum of the convex function is obtained where the first derivative is 0. This is satisfied for $V_S = V_T/2$. If $E(V)$ is strictly convex this minimizer is unique.

If E is a concave function, by using concavity twice we obtain

$$E(0) + E(V_T) \le E(V) + E(V_T - V), \tag{8}$$

for all $0 \le V \le V_T$, hence $V_S = 0$. If $E(V)$ is strictly concave the inequality is strict. □

Classical example A simple example of the concave case is an isolated water droplet in the absence of a solid phase. Since the energy minimizing configuration of a water drop in oil is a sphere, the energy graph obeys $E(V) = \sigma_{WO}(6\sqrt{\pi}V)^{2/3}$, so the graph is strictly concave. Consequently, any two spherical drops have a surface area greater than that of a single sphere with the combined volumes.

3.1.2 General $V - E$ graphs of DCPs

Both the hollow sphere and hollow cylinder DCPs have $V - E$ graphs with certain properties that lead to guaranteed bounds on the size of V_S. In this section we list the properties of the DCPs and prove theorems based on these properties. Our theorems require that $E(V) \in \mathbf{C}^1[0, \infty)$, which we assume for the rest of the paper (Fig. 8). For the proofs, it is easier to enumerate the properties of $E'(V)$ than $E(V)$. The properties of the hollow sphere are

Property A

(P1) For some $0 < V_1 < V_2$, $E'(V)$ strictly decreases for $0 \le V \le V_1$, strictly increases for $V_1 \le V \le V_2$ and again strictly decreases for $V_2 \le V$.
(P2) $\lim_{V\to\infty} E'(V) = 0$.
(P3) $E(V_2) - E(0) = \int_0^{V_2} E'(U)\mathrm{d}U \le 0$.

For such $E(V)$ the following theorem holds.

Theorem 3 *Consider two DCPs with the same $E(V)$ satisfying Property A above. For water of total volume V_T the following are true,*

1. *If $0 \le V_T \le V_1$, then $V_S = 0$ i.e. the other DCP contains all V_T.*
2. *The minimum energy volume of the DCP, $V_{\min} := \operatorname{argmin} E(V)$, satisfies $V_1 \le V_{\min} \le V_2$.*
3. *There exists a critical $V_b \ge V_2$, such that if $2V_b \le V_T$, then $V_{\min} \le V_S \le V_2$ i.e., a DCP contains a water volume in the range $[V_{\min}, V_2]$. Furthermore, $V_S \to V_{\min}$ as $V_T \to \infty$.*

The last result of the above theorem is important because it results in fairly uniform size volumes (between $V_{\min}$ and V_2) associated with a DCP. With many DCPs a similar result holds in which all but one DCP have a volume of water between these two bounds (cf. Fig. 14a). A DCP with a $V-E$ graph that yields V_1 close to V_2 and consequently $V_{\min}$ close to V_2 should trap a droplet with a specific volume between the two. This is a design feature of the DCP.

Proof We provide Fig. 8a as an example of a function that satisfies the given conditions. The first result follows from Theorem 2 since $E(V)$ is concave in the range $0 \le V \le V_1$. For the second result, we note that since $V_{\min} \ne 0$ by *(P3)*, $E'(V_{\min}) = 0$ holds. Since $E'(V_1) < 0$ by *(P1)* and *(P3)*, and $E'(V_2) > 0$ by *(P1)* and *(P2)*, there are at most two V that satisfy $E'(V) = 0$, one smaller than V_1 and the other between V_1 and V_2. It is straight forward to show that $V_{\min}$ is the latter.

The last result is proved as follows. Recall that V_S should satisfy (7) or either equal to 0. For $V_T \ge 2V_2$, property *(P1)* leads to $E'(V_T - V) > 0$, for $V < V_T/2$. For such total volumes, these two facts and *(P1)* restrict the possible values of V_S to 0, V_α, V_β, and $V_T/2$, where $0 < V_\alpha < V_1 < V_{\min} \le V_\beta \le V_2$. Note that

$E'(V_i) > 0$ for $V_i = V_\alpha, V_\beta,$ and $V_T/2$.

We show that $V_S = V_\beta$, provided that $V_T \ge 2V_b$ for some V_b.

1) Compare $V = 0$ and $V_{\min} \le V_\beta \le V_2$:
We show that

$$E(V_T) + E(0) - \left[E(V_T - V_\beta) + E(V_\beta)\right] \ge 0$$

for any $V_{\min} \le V_\beta \le V_2$ that satisfies (7). Notice that the left-hand side of the inequality is identical to the left-hand side of the following inequality:

$$\int_{V_T - V_\beta}^{V_T} E'(U)\mathrm{d}U - \int_0^{V_\beta} E'(U)\mathrm{d}U \ge -\int_0^{V_\beta} E'(U)\mathrm{d}U.$$

The above inequality holds since $E'(V) > 0$ for $V > V_2$. By combining $E'(V_\beta) > 0$ and *(P1)*, $E'(V) > 0$, for $V_\beta < V < V_2$. Together with *(P3)*,

$$-\int_0^{V_\beta} E'(U)\mathrm{d}U \ge -\int_0^{V_2} E'(U)\mathrm{d}U \ge 0. \tag{9}$$

2) Compare $0 < V_\alpha < V_1$ and $V_{\min} \le V_\beta \le V_2$:
Following the steps of the previous comparison, it is sufficient to show

$$-\int_{V_\alpha}^{V_\beta} E'(U)\mathrm{d}U \ge 0.$$

From $E'(V_\alpha) > 0$ and *(P1)*, $E'(V) > 0$ for $0 < V < V_\alpha$. Similar to (9), we deduce

$$-\int_{V_\alpha}^{V_\beta} E'(U)\mathrm{d}U \ge -\int_0^{V_2} E'(U)\mathrm{d}U \ge 0.$$

3) Compare $V = V_T/2$ and $V_{\min} \le V_\beta \le V_2$:
Again we want to show

$$-\int_{V_T/2}^{V_T - V_\beta} E'(U)\mathrm{d}U + \int_{V_\beta}^{V_T/2} E'(U)\mathrm{d}U \ge 0.$$

Note that by *(P1)*

$$-\int_{V_T/2}^{V_T - V_\beta} E'(U)\mathrm{d}U \ge -\int_{V_T/2}^{V_T - V_\beta} E'(V_T/2)\mathrm{d}U = -\int_{V_\beta}^{V_T/2} E'(V_T/2)\mathrm{d}U.$$

Therefore, showing

$$\int_{V_\beta}^{V_T/2} E'(U) - E'(V_T/2)\mathrm{d}U \ge 0$$

is sufficient. We now choose a V_b. By *(P1)* and *(P2)*, there exists a one to one correspondence between $V_{\min} \le W \le V_2$ and $V_2 \le V$ which satisfies $E'(W) = E'(V)$. We denote such W for V as $W(V)$. Note that, by $E'(V_{\min}) = 0$, $W(V) \to V_{\min}$ as $V \to \infty$. We choose a V_b that $W_b := W(V_b)$ satisfies

$$\int_{V_{\min}}^{W_b} E'(V_b)\mathrm{d}U \le \int_{W_b}^{V_b} E'(U) - E'(V_b)\mathrm{d}U. \tag{10}$$

The left-hand side and the right-hand side of the above inequality are represented as colored areas in Fig. 8a. Note that such V_b exists, since as $V_b \to \infty$, the left-hand side goes to 0, while the right-hand side increases from a positive value.
For $V_T \ge 2V_b$, $V_\beta \le W_b \le V_T/2$ holds and

$$\begin{aligned}
&\int_{V_\beta}^{V_T/2} E'(U) - E'(V_T/2)\mathrm{d}U \\
&\ge \int_{V_\beta}^{W_b} E'(U) - E'(V_b)\mathrm{d}U + \int_{W_b}^{V_T/2} E'(U) - E'(V_T/2)\mathrm{d}U \\
&\ge -\int_{V_\beta}^{W_b} E'(V_b)\mathrm{d}U + \int_{W_b}^{V_b} E'(U) - E'(V_T/2)\mathrm{d}U
\end{aligned}$$

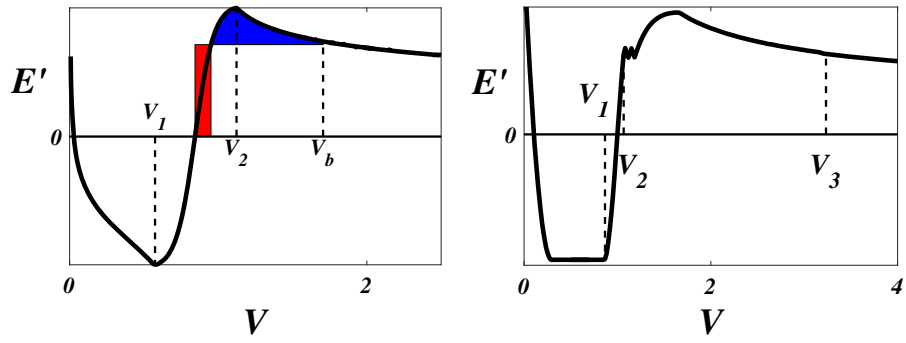

(a) $V - E'$ graph of hollow sphere **(b)** $V - E'$ graph of hollow cylinder

Fig. 8 $V - E'$ graph of the hollow sphere and hollow cylinder (Fig. 5 and 6). In (**a**), V_b is chosen so that (10) is satisfied. The area in light red and dark blue represents the value of the left- and right-hand side of (10) respectively. In (**b**) V_3 is chosen to correspond to Theorem 4

$$\geq -\int_{V_{\min}}^{W_b} E'(V_b)\mathrm{d}U + \int_{W_b}^{V_b} E'(U) - E'(V_b)\mathrm{d}U \geq 0.$$

The first and third inequality holds since $0 \leq E'(V_T/2) < E'(V_b)$. The second inequality holds since, $E'(V) \geq 0$ for $V_\beta \leq V \leq W_b$, and $E'(V) \geq E'(V_T/2)$ for $V_b \leq V \leq V_T/2$. The last inequality comes directly from (10). Since V_β satisfies $V_\beta = W(V_T - V_\beta)$, $V_\beta \to V_{\min}$ as $V_T \to \infty$.

□

Remark 1 1. For the case of the $V-E$ graph of a dropicle, as the volume increases, the water-oil surface asymptotes to a sphere and the effect of the DCP on the surface energy becomes negligible. Therefore the *(P2)* of the theorem

$$\lim_{V\to\infty} E'(V) \approx \lim_{V\to\infty} CV^{-1/3} = 0$$

is justified.

2. The proof demonstrates a tighter bound $V_{\min} \leq V_S \leq W_b$ regarding the last statement of the theorem.
3. We notice from the proof that V_b is small if $E'(V)$ increases rapidly between $V_{\min}$ and V_2. This condition has the added benefit that the range $[V_{\min}, V_2]$ is small.

Application to the hollow sphere The $V - E'$ graph of the hollow sphere is given in Fig. 8a with the values of V_1, V_2, and V_b. Theorem 3 predicts that when two hollow spheres and a large volume of water are present the energy minimizing distribution is one of the DCPs containing water of volume between $V_{\min}$ and V_2, and the other containing the rest. Note that the water-oil interfaces of both DCPs should have the same radius of curvature. This is due to the constant mean curvature condition of minimum energy surfaces (Sect. 2).

For the hollow cylinder, we relax the (P1) of Property A to

(P1′) There exists $0 < V_1 < V_2 < V_3$ so that $E'(V)$ decreases for $0 \leq V \leq V_1$, strictly increases for $V_1 \leq V \leq V_2$ and strictly decreases for $V_3 \leq V$. Also $E'(V) > 0$ for all $V > V_2$.

Based on this assumption, we prove a theorem with identical results.

Theorem 4 *If $E(V) \in \boldsymbol{C}^1[0,\infty)$ satisfy the conditions above, then the same conclusions of Theorem 3 hold.*

Proof We provide Fig. 8b as an example of a function that satisfies the conditions of the theorem. Most parts of the proof are similar to that of Theorem 3. Only the last conclusion needs to be modified. We assume that V_3,

satisfies $E'(V_3) < E'(V)$ for all $V_2 < V < V_3$. This is possible since, without loss of generality, we can choose a larger V_3 that has this property, by *(P1′)* and *(P2)*. Then for $V_T > 2V_3$, the possible values of V_S are the analogous 0, V_α, V_β, and $V_T/2$ in the previous proof. The comparisons between the possible values are similar except for the comparison between V_β and $V_T/2$, which we present below.

As in the previous proof we want to show

$$\int_{V_\beta}^{V_T/2} E'(U) - E'(V_T/2)\mathrm{d}U \geq 0$$

for $V_T > 2V_b$, for some V_b. Again for $V \geq V_3$ there is a function $W(V)$ such that $V_{\min} \leq W \leq V_2$ and $E'(W) = E'(V)$. We choose a $V_b \geq V_3$, so that the $W_b := W(V_b)$ satisfies

$$\int_{V_{\min}}^{W_b} E'(V_b)\mathrm{d}U \leq \int_{W_b}^{V_b} E'(U) - E'(V_b)\mathrm{d}U. \tag{11}$$

Such V_b exists since as $V_b \to \infty$ the left-hand side goes to 0 by $W_b \to V_{\min}$, while the right-hand side increases from a positive number by $E'(V) > E'(V_b)$ for $W_b < V < V_b$. The rest of the proof is similar. □

Application to the hollow cylinder Differentiating the $V-E$ graph of the hollow cylinder (Fig. 8b) shows Theorem 4 is applicable. If there are two such DCPs and a large enough volume of water, the energy minimum is obtained when a volume between $V_{\min}$ and V_2 is trapped in one of the DCPs.We note that the figure has some small oscillations in the E' graph at volumes just above V_2. This is due to the finite wall thickness of the DCP and is explained in more detail in the Appendix. Similar to the hollow sphere, all water-oil interfaces have the same radius of curvature.

3.2 Droplet splitting between many DCPs

In physical applications there are many DCPs in the system (Fig. 1). The minimum energy distribution of such system is the solution to the optimization problem

$$\overline{\mathbf{V}} = \mathrm{argmin}_{\substack{\Sigma V_i = V_T \\ V_i \geq 0}} \{\Sigma E(V_i)\}, \tag{12}$$

where $\overline{\mathbf{V}}$ is a vector with N entries representing N number of DCPs and V_i being the water volume in i-th DCP. Again the key is the concave and convex properties of $E(V)$.

Theorem 5 *For an energy function $E(V)$ and $0 < a < b$, the minimizer $\overline{\mathbf{V}}$ of (12) has the following properties.*

1. *If $E(V)$ is strictly concave on (a, b), then at most one of the entries of $\overline{\mathbf{V}}$ is in (a, b).*
2. *If $E(V)$ is strictly convex on $[a, b]$, then all the entries of $\overline{\mathbf{V}}$ on the domain $[a, b]$ are equal.*

Proof 1. Suppose not, i.e. there are two entries of $\overline{\mathbf{V}}$, $V_i \leq V_j$, that lie in (a, b). Then

$$E(V_i) + E(V_j) > E(V_i - \epsilon) + E(V_j + \epsilon)$$

for small enough ϵ. This contradicts that $\overline{\mathbf{V}}$ is the minimizer

2. Suppose not, i.e. there are two entries of $\overline{\mathbf{V}}$, $V_i < V_j$, which lie in $[a, b]$. Then

$$E(V_i) + E(V_j) > E(V_i + \epsilon) + E(V_j - \epsilon)$$

for small enough ϵ. This contradicts that $\overline{\mathbf{V}}$ is the minimizer

□

For the hollow sphere, the value of the distribution $\overline{\mathbf{V}}$ is proved rigorously, for sufficiently large total volume V_T.

Theorem 6 *If $E(V)$ satisfy Property A and $V_T \geq NV_b$, then $N-1$ entries of $\overline{\mathbf{V}}$ are between $V_{\min}$ and V_2.*

Proof By Theorem 5 (a) there is at most one entry of $\overline{\mathbf{V}}$ in the interval $(0, V_1)$ and likewise in (V_2, ∞); we denote these values as V_α and V_γ; (b) the entries in $[V_1, V_2]$ are equal which we denote as V_β; (c) the only other possible entry is 0. We show that V_β and V_γ are the only allowed values. By the total volume constraint there is an entry V_γ, since otherwise, all the entries of $\overline{\mathbf{V}}$ are less than V_b, and consequently $V_T < NV_b$.

Suppose that entry i and j of $\overline{\mathbf{V}}$ are 0 and V_γ respectively. Then $V_i + V_j = V_\gamma > 2V_b$, by a total volume argument similar to above. Applying Theorem 3 to the two-DCP system with DCP i and j shows that the distribution is not a minimum energy distribution. Therefore $\overline{\mathbf{V}}$ does not have any entries with value 0. The same argument applies to V_α. The fact that $V_{\min} \leq V_\beta \leq V_2$ follows from theorem 3 applied to V_β and V_γ. □

The theorems assure that the lowest energy state has all but one of the dropicles containing the same volume of water V_β. This minimizing volume occurs in the region where $E(v)$ is convex. This is numerically demonstrated in Sect. 4.3.

Note that in this section, we do not assume any geometric properties of the DCP other than the properties of the DCP's $V - E$ graph. Therefore the theorems not only hold for axisymmetric DCPs in Sect. 2 but also for any DCP with the appropriate properties [1].

4 Numerical simulations

In this section, we simulate pairwise interactions of a multi-DCP system, in which fluid can be exchanged in a pairwise fashion to minimize the pairwise surface energy. The method randomly chooses two DCPs, each with their own fluid volume, and redistributes the volume between the DCPs so as to minimize the surface energy of that two-DCP system. This process is repeated until the ensemble reaches a steady state.

First, we simulate the minimum energy distribution for two DCPs as a function of the total fluid volume. These simulations result in graphs that show how the fluid is distributed. These results are consistent with the rigorous theory from the previous section. In [1], actual dynamic splitting experiments are done in the laboratory showing that the theoretical results are a reasonable approximation. However dynamic splitting is known to sometimes lead to local energy minima rather than the global minimizer.

4.1 Simulation of a two-DCP system

First, we consider the interaction of two identical DCPs. This corresponds to solving the optimization problem in Sect. 3, which we restate here

$$V_S = \text{argmin}_{0 \leq V \leq V_T/2} \{E(V) + E(V_T - V)\}. \tag{13}$$

Once we specify $E(V)$, we can calculate $E(V) + E(V_T - V)$ for any given total volume V_T and find V_S. We plot V_S, as V_T varies, which we call the splitting graph. The splitting graphs of the hollow sphere and the hollow cylinder are shown in Fig. 9.

Fig. 9a is the splitting graph of the hollow sphere (whose energy curve is plotted in Fig. 5a). For small V_T, $V_S = 0$, while for large V_T, $V_{\min} \leq V_S \leq V_2$, which agrees with Theorem 3. Note that the theorem does not provide a prediction in the intermediate range (the domain that the droplets split evenly) which is straightforward to compute numerically. Fig. 9b is the splitting graph of the hollow cylinder (whose energy curve is plotted in Fig. 6a). Similar to the results of Fig. 9a the splitting graph agrees with Theorem 4.

The simulated splitting graph is compared to macroscale experiments [34]. The experiments use a hollow sphere and hollow cylinder DCP about 10mm in diameter, with densities of the fluids closely matched. The DCPs are initially close together sharing the same aqueous volume. They are slowly pulled apart to minimize the effect of dynamics. To plot the splitting graph we need the surface tension of the DCP. This is achieved by measuring the contact angle and using (3). The results are shown in Fig. 10 which the theoretical splitting graph and the experiment results agree considerably.

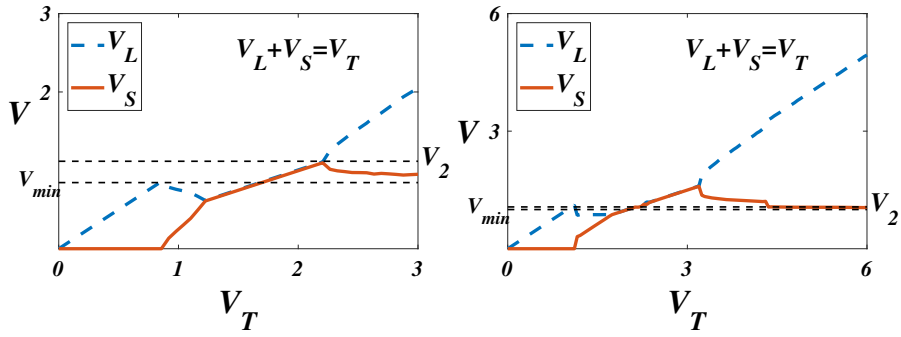

(a) Hollow sphere **(b)** Hollow cylinder

Fig. 9 Optimal splitting volume V_S of (13) with respect to V_T. **a** and **b** are the hollow spheres and hollow cylinders $V - E$ graph respectively (Fig. 5a and 6a). V_L and V_S indicate the larger and smaller volume of the droplets ($V_L = V_T - V_S$), while the dotted horizontal lines $V_{\min}$ and V_2 correspond to the volumes in theorems 3 and 4. The unit volumes are V_{1S} and V_{1C} respectively

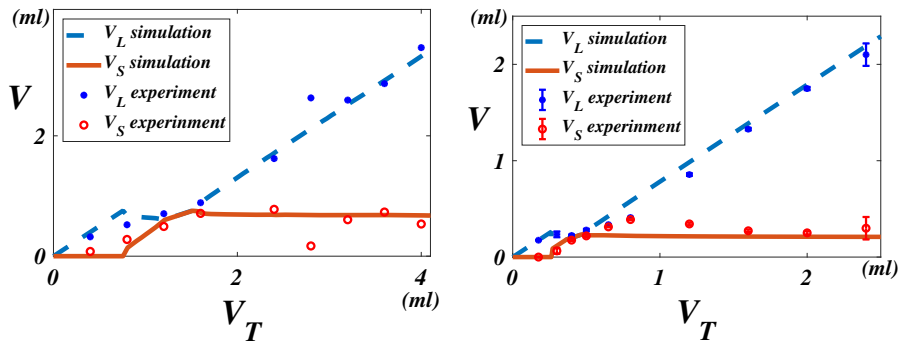

(a) Hollow sphere **(b)** Hollow cylinder

Fig. 10 Splitting graphs of the experiments and simulations [34]. V_L and V_S indicate the larger and smaller volume of the droplets. The lines correspond to the simulations and the dots correspond to the experimental data. Each dot indicates **a** one trial or **b** three trials, and the error bars correspond to one standard deviation of the data. The surface tensions for these graphs are matched to the materials in the experiments and therefore differ from the graphs in Fig. 9

In Fig. 9, the hollow cylinder has a more complicated splitting graph. For example, V_S of the hollow sphere never exceeds V_2, while the hollow cylinder does. Also, the minimum V_T required to guarantee $V_{\min} < V_S < V_2$ is smaller for the hollow sphere than the hollow cylinder. These properties are due to the finite thickness of the cylinder wall (see Appendix). Since the hollow sphere's splitting graph is simple, we focus on them in subsequent simulations.

4.2 Different geometries and surface tensions

In this section, we calculate the splitting graphs of the hollow sphere for different geometries and surface tensions. So far our computations are based on a specific shape of a hollow sphere DCP with fixed surface tension values. In this case, the splitting graph has two properties, (a) for small total volumes there is only one DCP that contains water and (b) for large total volumes there is a volume range that one DCP contains an amount of water volume within that range. We show that such results are robust in the sense that for a range of geometries and surface tensions the DCPs still possess these properties.

Fig. 11 shows the splitting graphs for spherical dropicles for three different geometries. The splitting graphs have the key features stated above. We also observe a trend that the difference between $V_{\min}$ and V_2 decreases as the opening of the DCP becomes smaller. This suggests that it may be desirable to have a hollow sphere with a small

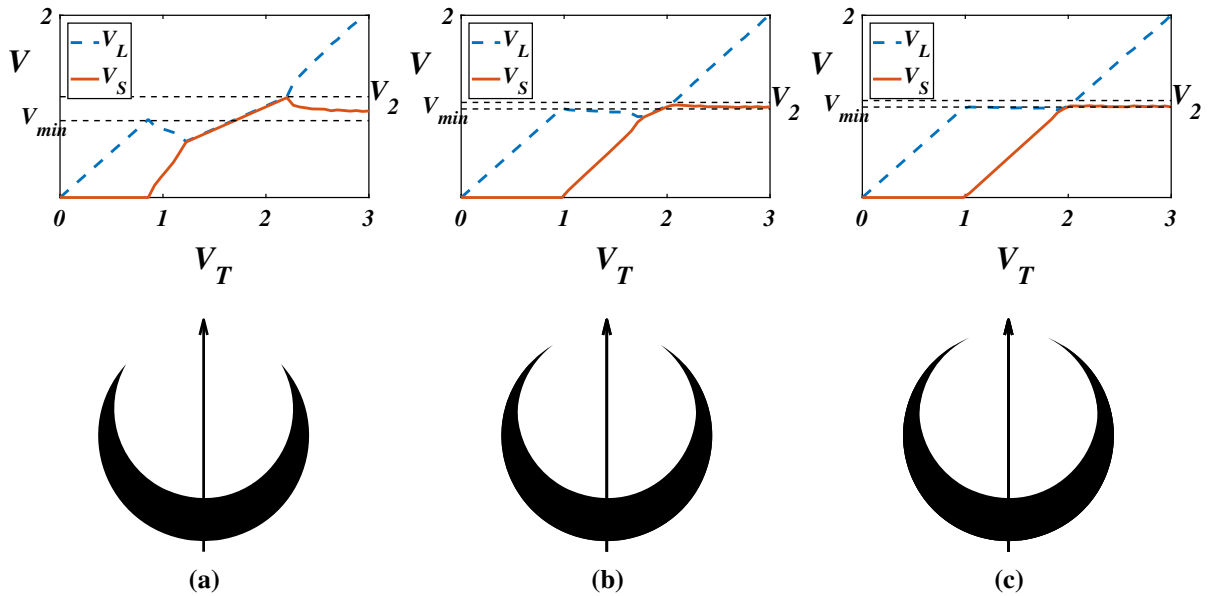

Fig. 11 Splitting graphs (top row) of various hollow sphere shapes (bottom row). The shape is chosen so that r and R are fixed and d is 0.5, 0.8 and 0.9 for (**a**), (**b**) and (**c**) respectively (Fig. 3b). The unit volume is V_{IS}

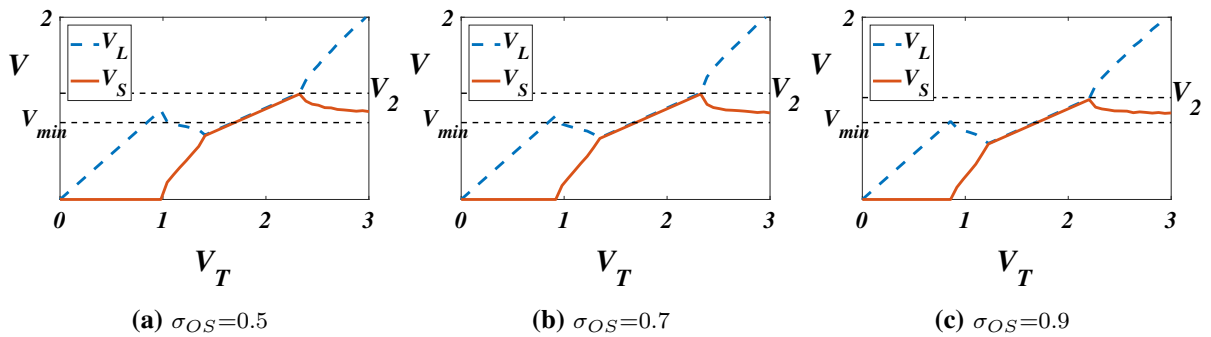

Fig. 12 Splitting graphs of hollow spheres with different surface tensions. Each graph has a different value of σ_{OS}, the oil-solid surface tension, which are 0.5, 0.7 and 0.9 for (**a**), (**b**) and (**c**) respectively. The other surface tensions are fixed as $\sigma_{WS} = 0.1$ and $\sigma_{WO} = 1$. The shape of the DCP is that of Fig. 11d and the unit volume is V_{IS}

opening to create more uniform volumes amongst a set of DCPs. However, practically if the opening is too small, it might be difficult for the fluid to exchange readily and the tip of the DCP might be fragile.

Fig. 12 shows the splitting graphs as we change the surface tension between oil and solid, σ_{OS}, within the range of partial wetting. Such changes have almost no effect on the splitting graph, compared to the changes in the shape of the DCP. This indicates that experiments are expected to behave similarly for a range of solid and fluid materials with different surface tensions.

4.3 Simulations of a multi-DCP systems

For the multi-DCP case we need to solve the optimization problem (12) which we restate here,

$$\overline{\mathbf{V}} = \text{argmin}_{\substack{\Sigma V_i = V_T \\ V_i \geq 0}} \{\Sigma E(V_i)\}. \tag{14}$$

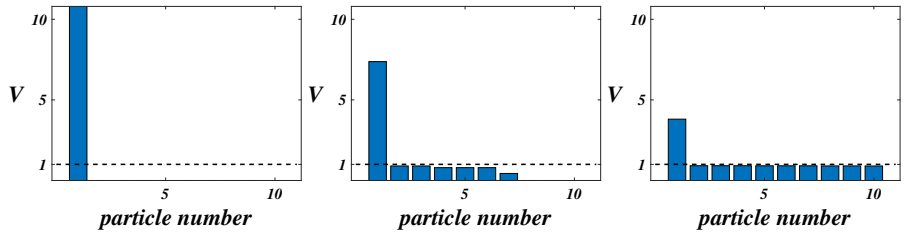

Fig. 13 The volume in each of the 10 hollow sphere DCPs (Fig.5) as they interact according to the randomized procedure. **a** is the initial distribution. **b** shows the result after 100 interactions. **c** shows the end state after 1000 interactions. The unit volume is V_{IS}

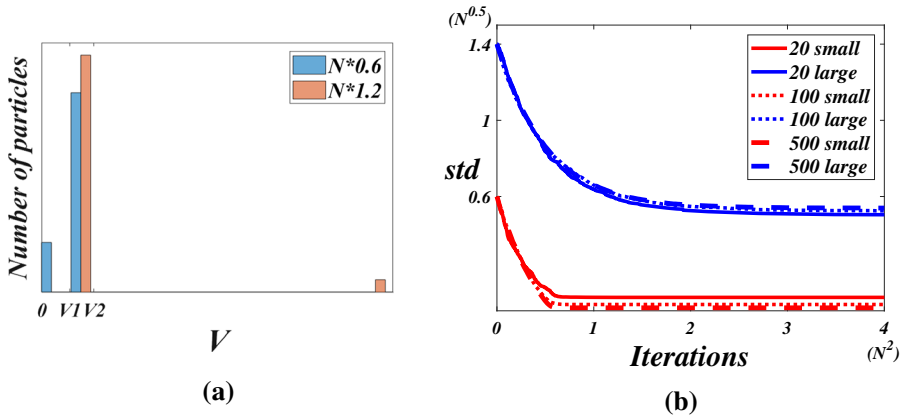

Fig. 14 Simulation results on multiple hollow sphere DCPs (Fig.5). **a** is a histogram of the final distribution of a 20 spherical DCP system. The total volumes of the blue and orange distribution are $0.6N$ and $1.2N$ respectively, where N is the number of DCPs. **b** plots the standard deviation of the volume vector $\mathbf{V}$ with respect to the number of pairwise interactions. The red and blue lines correspond to the total volume of $0.6N$ (small) and $1.4N$ (large) respectively, where $N = 20$, 100, and 500. Each line is the mean of 20 simulations. The number of interactions is normalized by N^2, and the standard deviation is normalized by $V_{IS}\sqrt{N}$

If $E(V)$ satisfies property A, we predict that all except one of the nonzero entries of $\overline{\mathbf{V}}$ have the same volume, as long as we start with sufficiently large total volume. Here we show numerically that this lowest energy state is achieved by repeated random pairwise interactions, outlined below.

Randomized procedure

1. Initialize volume vector $\mathbf{V}$ so that $V_1 = V_T$ and $V_k = 0$ for $k \geq 2$.
2. Repeat the following until a final distribution of $\mathbf{V}_F$ is obtained.
   (a) Choose DCPs i and j at random and solve the two DCP optimization (13), for $V_T = V_i + V_j$.
   (b) Update $V_i = V_S$ and $V_j = V_T - V_S$.

This randomized interaction is the simplest model to imitate the exchanging of fluid between dropicles colliding at random during an agitation process that leads to emulsification. The detailed statistical mechanics of this problem is further studied in [34]. For the geometries considered here, exclusively pairwise interactions are reasonable since not many dropicles can interact simultaneously with any other dropicle at a given time.

Figure. 13 shows how the distribution changes as we increase the number of interactions. The volume that was initially attached to one DCP distributes to other DCPs as they interact. Once the system reaches state Fig. 13a the minimum energy distribution is achieved (Theorem 6) and any additional interaction of the dropicles does not change the final distribution [34]. During the simulation, the water-oil interfaces of the dropicles do not need to have the same radius of curvature. However once the final distribution $\mathbf{V}_F$ is achieved, the radius of curvature is identical among the dropicles.

The final distributions $\mathbf{V}_F$ of a 20 DCP system are shown in Fig. 14a. The colors of the histogram represent simulations of total volumes $20 * 0.6$ and $20 * 1.2$, respectively. For the smaller total volume (blue), the non-empty dropicles each contain equal volume of water. For the larger total volume (orange), there is one dropicle with an excess amount of water while all the other dropicles contain equal volume. These results agree with Theorems 5 and 6.

Another question that the randomized procedure raises is how many interactions are needed to achieve $\mathbf{V}_F$. In physical experiments, this corresponds to how much mixing is needed to distribute the water between all the DCPs. We numerically calculate the standard deviation of $\mathbf{V}$ as we increase the number pairwise of interactions for different number of DCPs N and total volumes $0.6N$ and $1.4N$ (Fig. 14b). We observe a decreasing trend and that it flattens out once $\mathbf{V} = \mathbf{V}_F$. Note that for systems with total volume $1.4N$, more number of interactions are required to achieve a final distribution. This is because the system with total volume $0.6N$ needs to fill fewer DCPs compared to that with a total volume $1.4N$. Also, notice that the curves with different numbers of DCPs overlap for total volume of $0.6N$ and $1.4N$. This indicates that there is a general trend that determines the number of interactions.

5 Conclusion

This paper develops a fundamental theory for the distribution of fluid between microscale "dropicles" in the case of axisymmetry. Previous work on the minimal energy state of multiphase fluid-solid interactions was limited to the classic problem of catenoidal liquid bridges [29]. This work develops the necessary theory for modern "dropicle" interactions that are of particular interest in emerging "lab on a particle" technologies [1,9]. Using the generated minimal energy volume curves, we predict that randomized pairwise interactions between multiple dropicles have a long-time equilibrium distribution with effectively uniform water volumes adhering to each DCP, except for a sole dropicle with excess volume.

Comparing our simulations to the experimental data we find that they agree to a large extent (Fig. 10). However, there are assumptions in our model that contribute to the discrepancy between simulations and physical experiments. For example, two-DCP experiments may achieve a local energy minimum rather than a global one, including the possibility of the formation of satellite drops as shown in experiments on capillary breakup [38].

As we have explored in Sect. 4.2, as long as the shape and surface tension of the DCPs are within the range of physical interest, we get a water droplet of size within the range $[V_{\min}, V_2]$, as specified in Theorem 3 and 4. Here we consider minimizing the interval size $[V_{\min}, V_2]$ to better uniformize the water droplet size. Likewise minimizing V_b in Theorem 3 and 4 reduces the size of the excess volume needed to guarantee this distribution. Further work could optimize a DCP according to these two measures.

For large total volumes, the lowest energy configuration of the multiple DCP system consists of $N-1$ dropicles with the same volume and the N-th one with the remaining large volume. This type of volume distribution is observed in fluid-solid interfacial systems with multiple orifices [31–33]. In those systems the energy minimization solution is comprised of partial spheres bulging out from the orifices. For large total volumes, the stable distribution of fluid on each orifice is $N-1$ of them with the same small volume while the last orifice has a large drop attached. The difference between the two minimizers is the limit of the smaller volume, V_S, as the total volume, V_T, increases; for the orifices, $V_S \to 0$, while in the DCP system the minimizing configuration has a non-zero lower bound $V_{\min}$. In fact, this limiting non-zero volume is the main feature of the system design in order to create uniform droplet sizes - as miniature test tubes for applications like biological assays [1].

We also investigated the number of interactions needed to obtain the final distribution. This is related to the degree of physical mixing required to achieve a good distribution in practice. We propose the standard deviation of the vol-

ume vector **V** (Fig. 14b) as a way of determining if **V** is a final distribution. However, this method requires expensive computations. Instead, we would like an inexpensive method of calculating the required number of interactions.

Although the DCPs are not connected physically, two DCPs, after they interact, have a water-oil interface with identical radius of curvature. In a multi-DCP system, the radius of curvature of the interface of each dropicle can be different. For the fixed distribution however, the radius of curvature of the interfaces is the same.

The analysis in this paper relies exclusively on the $E(V)$ graph. Therefore it easily generalizes to non-axisymmetric DCPs such as the ones described in [1,8]. This is advantageous since many axisymmetric shapes are difficult to manufacture at the microscale. As long as the DCPs have the properties in theorem 3 or 4, we obtain analogous minimum energy distributions to the axisymmetric case.

Acknowledgements This work is supported by the Simons Math + X project (510776) and the National Science Foundation Grant (1648451). Fig. 10 was generated by an REU team during the summer of 2019 supported by the NSF (DMS-1659676). The team members include Bernardo Hernandez Adame, Ryan Shijie Du, Lily Liu, Simon Ng, Hansell Perez, Sneha Sambandam, Claudia Falcon. We thank the reviewers for helpful comments that improved the manuscript.

Appendix

In Fig 8b the E' graph has four critical points for volumes $\leq V_2$, due to the hollow cylinder having a wall of finite width. Here we explain how the minimum energy configuration changes between the four critical points as the water volume increases. An enlarged figure with the critical points labeled is shown in Fig. 15.

As the volume captured by the DCP increases from 1 to V_2 (configuration A) both top and bottom oil–water interfaces bulge symmetrically. However, for volumes between A and B, this symmetric configuration is no longer the energy minimum. Rather, the minimum configuration is asymmetric with one side (the bottom side in the figure) having the contact line between the outer and inner edges and on the other side (the top side) the contact line is fixed on the inner edge.

The contact line on the bottom reaches the outer edge for a specific volume designated by the notation B in Fig. 15. As the volume increases further, the contact lines are fixed again while the free surfaces bulge out. Between configurations C and D, the top contact line moves to the outer edge (see configuration D) after which the two interfaces bulge symmetrically, for increasing V. Note that these changes involve a symmetry breaking between the top and bottom of the cylinder. There is another critical point in the $E' - V$ graph at $V \approx 1.7$ (Fig. 8b) that corresponds to a symmetry breaking in which for larger values of V the lowest energy surface has a sphere protruding

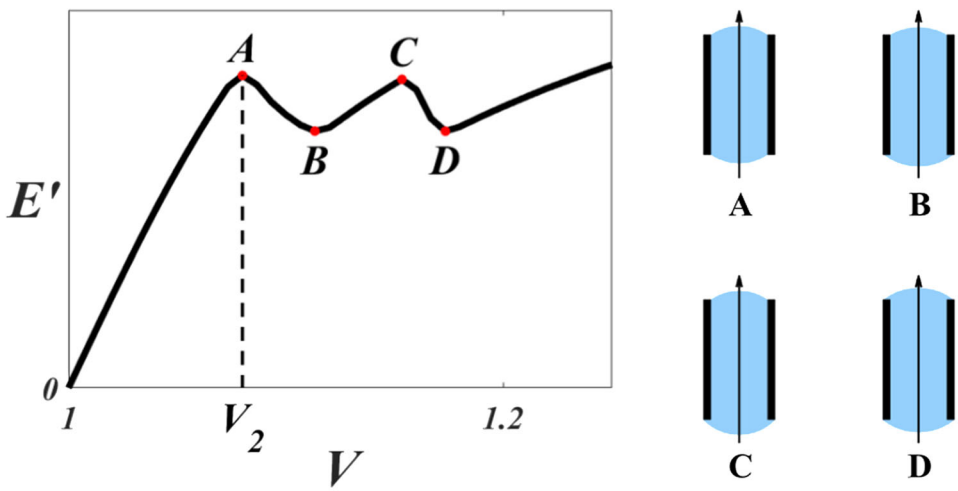

Fig. 15 An enlarged graph of Fig. 8b and cross section configurations at each critical point

from one end and a smaller spherical cap (with the same radius of curvature) protruding from the other end. We note that this phenomenon is similar to the configuration of droplets deposited on an orifice [39].

References

1. Chueh-Yu W, Ouyang M, Wang B, de Rutte J, Joo A, Jacobs M, Ha K, Bertozzi AL, Di Carlo D (2020) Monodisperse drops templated by 3d-structured microparticles. Sci Adv 6(45)
2. Kawakatsu T, Kikuchi Y, Nakajima M (1997) Regular-sized cell creation in microchannel emulsification by visual microprocessing method. J Am Oil Chem Soc 74(3):317–321
3. Anna SL, Bontoux N, Stone HA (2003) Formation of dispersions using "flow focusing" in microchannels. Appl Phys Lett 82(3):364–366
4. Tan Y-C, Cristini V, Lee AP (2006) Monodispersed microfluidic droplet generation by shear focusing microfluidic device. Sens Actuators B 114(1):350–356
5. Lu H-S, Bottausci F, Fowler JD, Bertozzi AL, Meinhart C et al (2008) A study of EWOD-driven droplets by PIV investigation. Lab Chip 8(3):456–461
6. Nelson WC, Jin C, Kim CJ (2012) Droplet actuation by electrowetting-on-dielectric (EWOD): a review. J Adhes Sci Technol 26(12–17):1747–1771
7. Xi H-D, Zheng H, Guo W, Gañán-Calvo AM, Ai Y, Tsao C-W, Zhou J, Li W, Huang Y, Nguyen N-T et al (2017) Active droplet sorting in microfluidics: a review. Lab Chip 17(5):751–771
8. Destgeer G, Ouyang M, Wu CY, Di Carlo D (2020) Fabrication of 3d concentric amphiphilic microparticles to form uniform nanoliter reaction volumes for amplified affinity assays. Lab Chip
9. de Rutte J, Dimatteo R, Archang MM, van Zee M, Koo D, Lee S et al (2022) Suspendable hydrogel nanovials for massively parallel single-cell functional analysis and sorting. ACS nano
10. Destgeer G, Ouyang M, Di Carlo D (2021) Engineering design of concentric amphiphilic microparticles for spontaneous formation of Picoliter to nanoliter droplet volumes. Anal Chem 93(4):2317–2326
11. Bernoff AJ, Bertozzi AL, Witelski TP (1998) Axisymmetric surface diffusion: dynamics and stability of self-similar Pinchoff. J Stat Phys 93(3–4):725–776
12. Bostwick JB, Steen PH (2015) Stability of constrained capillary surfaces. Ann Rev Fluid Mech 47
13. Mason G, Clark WC (1965) Liquid bridges between spheres. Chem Eng Sci 20(10):859–866
14. Pitois O, Moucheront P, Chateau X (2000) Liquid bridge between two moving spheres: an experimental study of viscosity effects. J Colloid Interface Sci 231(1):26–31
15. Rabinovich YI, Esayanur MS, Moudgil BM (2005) Capillary forces between two spheres with a fixed volume liquid bridge: theory and experiment. Langmuir 21(24):10992–10997
16. Slobozhanin LA, Alexander JID, Patel VD (2002) The stability margin for stable weightless liquid bridges. Phys Fluids 14(1):209–224
17. Strube D (1992) Stability of a spherical and a catenoidal liquid bridge between two parallel plates in the absence of gravity. Microgravity fluid mechanics. Springer, New York, pp 263–269
18. Vogel TI (1987) Stability of a liquid drop trapped between two parallel planes. SIAM J Appl Math 47(3):516–525
19. Vogel TI (1989) Stability of a liquid drop trapped between two parallel planes II: general contact angles. SIAM J Appl Math 49(4):1009–1028
20. Zhou L (1997) On stability of a catenoidal liquid bridge. Pac J Math 178(1):185–198
21. Erle MA, Gillette RD, Dyson DC (1970) Stability of interfaces of revolution with constant surface tension-the case of the catenoid. Chem Eng J 1(2):97–109
22. Gillette RD, Dyson DC (1971) Stability of fluid interfaces of revolution between equal solid circular plates. Chem Eng J 2(1):44–54
23. Slobozhanin LA, Shevtsova VM, Alexander JID, Meseguer J, Montanero JM (2012) Stability of liquid bridges between coaxial equidimensional disks to axisymmetric finite perturbations: a review. Microgr Sci Technol 24(2):65–77
24. Russo MJ, Steen PH (1986) Instability of rotund capillary bridges to general disturbances: experiment and theory. J Colloid Interface Sci 113(1):154–163
25. Lowry BJ, Steen PH (1997) Stability of slender liquid bridges subjected to axial flows. J Fluid Mech 330:189–213
26. Lowry BJ, Steen PH (1995) Capillary surfaces: stability from families of equilibria with application to the liquid bridge. Proc R Soc Lond A 449(1937):411–439
27. Gillette RD, Dyson DC (1972) Stability of axisymmetric liquid–fluid interfaces towards general disturbances. Chem Eng J 3:196–199
28. Slobozhanin LA, Perales JM (1996) Stability of an isorotating liquid bridge between equal disks under zero-gravity conditions. Phys Fluids 8(9):2307–2318
29. Akbari A, Hill RJ, van de Ven TGM (2015) Catenoid stability with a free contact line. SIAM J Appl Math 75(5):2110–2127
30. Myshkis AD, Babskii VG, Kopachevskii ND, Slobozhanin LA, Tyuptsov AD, Wadhwa RS (1987) Low-gravity fluid mechanics. Translated from the Russian by Wadhwa, RS, XIX, 583 pp. 218 figs. Springer, Berlin, pp 218
31. Wente HC (1999) A surprising bubble catastrophe. Pac J Math 189(2):339–375
32. Vogel MJ, Steen PH (2010) Capillarity-based switchable adhesion. Proc Natl Acad Sci 107(8):3377–3381

33. Hagen TC, Steen PH (2019) Volume scavenging of networked droplets. Physica D 394:1–15
34. Du RS, Liu L, Ng S, Sambandam S, Adame BH, Perez H, Ha K, Falcon C, de Rutte J, Di Carlo D et al (2021) Statistical energy minimization theory for systems of drop-carrier particles. Phys Rev E 104(1):015109
35. Ascher UM, Petzold LR (1998) Computer methods for ordinary differential equations and differential-algebraic equations. Siam 61
36. Neukirch S, Antkowiak A, Marigo J-J (2013) The bending of an elastic beam by a liquid drop: a variational approach. Proc R Soc A 469(2157):20130066
37. Brubaker ND (2019) Two-dimensional capillary origami with inextensibility and free triple-contact points. SIAM J Appl Math 79(2):572–593
38. Tjahjadi M, Stone HA, Ottino JM (1992) Satellite and subsatellite formation in capillary breakup. J Fluid Mech 243:297–317
39. Hanysz B, Nowicki W (2019) The capillary bistable switch constrained by pinning/wetting angles as a sensor of pressure. Eur Phys J E 42(9):1–5